



# CHORUS

This is the accepted manuscript made available via CHORUS. The article has been published as:

## Enormous electron-electron scattering in the filled-cage cubic compound $\text{Ba}_{10}\text{Ti}_{24}\text{Bi}_{39}$

Fei Han, Jin-Ke Bao, Christos D. Malliakas, Mihai Sturza, Yongping Du, Duck Young Chung, Xiangang Wan, and Mercouri G. Kanatzidis

Phys. Rev. Materials **3**, 105001 — Published 7 October 2019

DOI: [10.1103/PhysRevMaterials.3.105001](https://doi.org/10.1103/PhysRevMaterials.3.105001)

# Enormous Electron-Electron Scattering in the Filled-Cage Cubic Compound $\text{Ba}_{10}\text{Ti}_{24}\text{Bi}_{39}$

Fei Han,<sup>1,2</sup> Yongping Du,<sup>3</sup> Christos D. Malliakas,<sup>1,4</sup> Mihai Sturza,<sup>1,5</sup> Jin-Ke Bao,<sup>1</sup> Duck Young Chung,<sup>1</sup> Xiangang Wan,<sup>3</sup> and Mercouri G. Kanatzidis<sup>1,4,\*</sup>

*1. Materials Science Division, Argonne National Laboratory, Argonne, Illinois 60439, United States*

*2. Department of Nuclear Science and Engineering, Massachusetts Institute of Technology, Cambridge, MA 02139, United States*

*3. National Laboratory of Solid State Microstructures, School of Physics, Collaborative Innovation Center of Advanced Microstructures, Nanjing University, Nanjing 210093, China*

*4. Department of Chemistry, Northwestern University, Evanston, Illinois 60208, United States*

*5. Leibniz Institute for Solid State and Materials Research Dresden IFW, Institute for Solid State Research, 01069 Dresden, Germany*

## ABSTRACT

The cubic intermetallic compound  $\text{Ba}_{10}\text{Ti}_{24}\text{Bi}_{39}$  has a  $\text{Ba}_6\text{Bi}_{16}$  polyhedral cage with a Bi guest atom encapsulated inside. The compound can be formulated as  $\text{Ba}_5\text{Ti}_{12}\text{Bi}_{19+x}$  when  $x$  signifies the extra Bi atoms filling cages. It crystallizes in a complex non-centrosymmetric cubic structure in space group  $P-43m$  with cell parameter  $a = 12.6881(8)$  Å. The guest Bi atoms distribute diffusely in the cages and seem to play a role in stabilizing the crystal structure. The magnetic susceptibility of this compound shows a weak temperature dependence with a positive slope coefficient. The charge transport properties as a function of temperature exhibit two competing components which are in charge of positive and negative magnetoresistances. Electronic band structure calculations reveal the complex multiband hybridization of Ti/Bi orbitals near the Fermi surface, which may play a role in the enormous electron-electron scattering in this material evidenced by the large Kadowaki-Woods ratio.

Corresponding Author: \*E-mail: [m-kanatzidis@northwestern.edu](mailto:m-kanatzidis@northwestern.edu)

## INTRODUCTION

Bismuth is unique among metallic elements as it is located closest to the border of metal and semiconductor, possesses the largest degree of spin-orbit coupling and has the smallest Fermi surface among all the non-radioactive elements. When bismuth forms intermetallics, it can adopt bonding that spans the entire spectrum between metallic and ionic. The variety of the bonding characters in bismuthides results in electronic properties of from semiconductor to semi-metal to metal. Furthermore, the strong spin-orbit coupling (SOC) effects can cause splitting of electronic bands giving rise to topologically nontrivial electronic structures.[1,2] During the past several years, several novel phenomena have been reported in bismuthides, including superconductivity in  $\text{NiBi}_3$ ,[3]  $\text{Ca}_{11}\text{Bi}_{10-x}$ ,[4]  $\text{NaBi}$ [5] and  $\text{BaBi}_3$ ,[6] Dirac fermions in  $\text{Na}_3\text{Bi}$ ,[7-9]  $Ae\text{MnBi}_2$  ( $Ae = \text{Ca}, \text{Sr}, \text{Ba}$ )[10-14] and  $\text{LaAgBi}_2$ ,[15] possible topological superconductivity in  $\beta\text{-PdBi}_2$ [16] and  $R\text{PdBi}$  ( $R =$  rare earth),[17] and topological semi-metallicity and large magnetoresistance in  $\text{LaBi}$ . [18-20] These discoveries motivate the further exploration of new phases. Some new compounds such as the superconductors  $\text{CoBi}_3$ ,[21]  $\text{Cu}_{11}\text{Bi}_7$ [22] and  $\text{LaPd}_{1-x}\text{Bi}_2$ ,[23,24] the antiferromagnetic Kondo lattice compound  $\text{CePd}_{1-x}\text{Bi}_2$ ,[25] their analogs  $R\text{Ni}_{1-x}\text{Bi}_{2+y}$  ( $R = \text{La-Nd}, \text{Sm}, \text{Gd-Dy}$ )[26] and  $R\text{AuBi}_2$  ( $R = \text{La-Nd}, \text{Sm}, \text{Gd}$ ),[27,28] and the first iron-bismuth bonding material  $\text{FeBi}_2$ [29] are notable examples. Recently, the synthesis and characterization of  $\text{Ba}_{10}\text{Ti}_{24}\text{Bi}_{39}$  was reported to form from Bi flux.[30]

In this paper we investigate this unusual ternary bismuthide  $\text{Ba}_{10}\text{Ti}_{24}\text{Bi}_{39}$ . The formulation  $(\text{Ba}^{2+})_{10}(\text{Ti}^{4+})_{24}(\text{Bi}^{3-})_{39}$  is almost electronically charge balanced suggesting  $\text{Ba}_{10}\text{Ti}_{24}\text{Bi}_{39}$  is possibly a Zintl phase.[31]  $\text{Ba}_{10}\text{Ti}_{24}\text{Bi}_{39}$  adopts a novel filled-cage structure with a disordered guest encapsulated in the cage.[30] We report here that this compound displays a two-component behavior in

magnetoresistance, and an enormous degree of electron-electron scattering in its electronic transport.

## EXPERIMENTAL SECTION

**Sample Preparation.** We grew the  $\text{Ba}_{10}\text{Ti}_{24}\text{Bi}_{39}$  crystals from Bi flux. Approximately total of 3 g of Ba ingot, Ti powder and Bi granules in the molar ratio of 5:12:100 were mixed and loaded in an alumina crucible. The handling of chemicals was performed in a glovebox with an argon atmosphere (both  $\text{H}_2\text{O}$  and  $\text{O}_2$  are limited below 0.1 ppm). The alumina crucible with its opening covered by a stainless steel sieve was sealed in an evacuated silica tube. The silica tube was heated to 900 °C in a box furnace and kept at 900 °C for 24 h. Then a slow-cooling process from 900 to 400 °C was carried out during 100 h. At 400 °C the excess Bi flux was canted by centrifugation. Polyhedral crystals with metallic luster (as shown in Figure 1(a)) were collected on the stainless steel sieve. The obtained air-sensitive crystals had a typical dimension of  $2 \times 2 \times 2 \text{ mm}^3$ . The yield was near 50% based on the amount of Ba and Ti. Due to the possible reaction between Ti metal and alumina crucible,[32] we also grew the  $\text{Ba}_{10}\text{Ti}_{24}\text{Bi}_{39}$  single crystals by directly loading the mixtures into the silica tube. The results of those two methods are similar to each other except that we got a minor phase  $\epsilon\text{-TiO}$ [33] with a needle shape when the alumina crucible for crystal growth was used, see Figure S5 in supplementary materials (SM).[34] To avoid possible interference of the residual Bi flux on property measurements, the crystals were cleaved with a blade inside a glovebox and only the inner parts of the crystals were used for structural and physical property characterization.

**Single-crystal X-ray Diffraction.** A piece of well-formed crystal was picked out with the help of an optical microscope located in the glovebox. The crystal was

fixed in a glass capillary with the Dow Corning high vacuum grease. Then the capillary was evacuated and flame-sealed to keep the crystal stable. Single-crystal X-ray diffraction measurement was done on a STOE IPDS-2T diffractometer at room temperature. Data reduction, integration, and absorption correction were performed with the software X-Area,[35] and the structure was solved by the direct methods and refined using the SHELXTL software.[36] The resulting structure parameters are listed in Table 1, 2 below and Table S1 in SM.[34]

**Table 1.** Crystal data and structure refinement for Ba<sub>10</sub>Ti<sub>24</sub>Bi<sub>39</sub> at 293(2) K.

Empirical formula	Ba <sub>10</sub> Ti <sub>24</sub> Bi <sub>39</sub>
Formula weight	10673.22
Temperature	293(2) K
Wavelength	0.71073 Å
Crystal system	cubic
Space group	P-43m
Unit cell dimensions	$a = 12.6787(4) \text{ \AA}, \alpha = 90.00^\circ$ $b = 12.6787(4) \text{ \AA}, \beta = 90.00^\circ$ $c = 12.6787(4) \text{ \AA}, \gamma = 90.00^\circ$
Volume	2038.09(11) Å <sup>3</sup>
Z	1
Density (calculated)	8.696 g/cm <sup>3</sup>
Absorption coefficient	90.739 mm <sup>-1</sup>
F(000)	4325
Crystal size	0.1×0.1×0.1 mm <sup>3</sup>
θ range for data collection	2.78 to 24.98°

Index ranges	-15<=h<=15, -15<=k<=15, -15<=l<=15
Reflections collected	13043
Independent reflections	732 [ $R_{\text{int}} = 0.0562$ ]
Completeness to $\theta = 24.98^\circ$	99.5%
Refinement method	Full-matrix least-squares on $F^2$
Data / restraints / parameters	732 / 0 / 47
Goodness-of-fit	1.226
Final R indices [ $>2\sigma(I)$ ]	$R_{\text{obs}} = 0.0289$ , $wR_{\text{obs}} = 0.0577$
R indices [all data]	$R_{\text{all}} = 0.0311$ , $wR_{\text{all}} = 0.0584$
Largest diff. peak and hole	2.548 and -3.545 e $\cdot\text{\AA}^{-3}$

---

$R = \frac{\sum ||F_o| - |F_c||}{\sum |F_o|}$ ,  $wR = \left\{ \frac{\sum [w(|F_o|^2 - |F_c|^2)^2]}{\sum [w(|F_o|^4)]} \right\}^{1/2}$  and calc  
 $w = 1 / [\sigma^2(F_o^2) + (0.0324P)^2 + 0.2990P]$  where  $P = (F_o^2 + 2F_c^2) / 3$

**Table 2.** Atomic coordinates ( $\times 10^4$ ) and equivalent isotropic displacement parameters ( $\text{\AA}^2 \times 10^3$ ) for  $\text{Ba}_{10}\text{Ti}_{24}\text{Bi}_{39}$  at 293(2) K with estimated standard deviations in parentheses.

Label	$x$	$y$	$z$	Occupancy	$U_{\text{eq}}^*$
Ti(1)	1608(3)	1608(3)	3285(4)	1	18(1)
Ti(2)	1827(3)	5000	0	1	16(1)
Ba(1)	8356(2)	8356(2)	8356(2)	1	26(1)
Ba(2)	1766(2)	5000	5000	1	36(1)
Bi(1)	3342(1)	3342(1)	120(1)	1	17(1)
Bi(2)	3225(1)	3225(1)	3225(1)	1	20(1)
Bi(3)	3560(1)	0	0	1	16(1)
Bi(4)	2194(1)	2194(1)	5478(1)	1	19(1)
Bi(5)	1113(1)	1113(1)	1113(1)	1	19(1)
Bi(6)	5000	5000	5000	0.70(3)	191(12)

Bi(6')	5878(9)	4122(9)	4122(9)	0.074(7)	22(7)
--------	---------	---------	---------	----------	-------

\* $U_{eq}$  is defined as one third of the trace of the orthogonalized  $U_{ij}$  tensor.

**Magnetization Measurements.** Magnetization measurements for  $Ba_{10}Ti_{24}Bi_{39}$  were carried out on a commercial Quantum Design magnetic property measurement system (MPMS3). A crystal (sample Q1) of 90.6 mg selected from the batch which was grown in a silica tube was directly mounted on a quartz sample holder with a negligible amount of GE varnish. The data presented in the main text are from the sample Q1. Another crystal (sample A1) of 66.3 mg grown in the alumina crucible were also checked for its magnetic properties, whose results were presented in SM. [34]

**Resistivity and Magnetoresistance Measurements.** After the crystals were cleaved in the glovebox, a piece of bar-shaped crystal with clean surface was selected for resistivity and magnetoresistance measurements. The measurements were carried out on a Quantum Design physical property measurement system (PPMS) with magnetic fields up to 9 T. The contacts in four-probe geometry were made with gold wires and silver paint under the protection of glovebox. For the magnetoresistance measurements, the field was applied approximately perpendicular to the longitudinal dimension of the crystal.

**Specific Heat Measurements.** We employed the thermal relaxation technique to perform the specific heat measurement on the Quantum Design PPMS. N-grease was used as heat-conducting medium.

**Band Structure Calculations.** Band structure calculations for  $Ba_{10}Ti_{24}Bi_{39}$  were performed with the Vienna *ab initio* simulation package (VASP).[37,38] The results were obtained by using the generalized gradient approximation (GGA) Perdew-Becke-Erzenhof (PBE) function.[39] An energy cutoff of 400 eV was adopted for

the plane-wave expansion of the electronic wave function and the energy convergence criterion was set to  $10^{-5}$  eV. To sample the Brillouin zone, appropriate k-point meshes of  $(9 \times 9 \times 9)$  were used for calculations. The spin-orbit coupling (SOC) effect was taken into account by the second variation method.[40]

## RESULTS AND DISCUSSION

**Crystal Structure.**  $\text{Ba}_{10}\text{Ti}_{24}\text{Bi}_{39}$  (also formulated as  $\text{Ba}_5\text{Ti}_{12}\text{Bi}_{19+x}$ ) crystallizes in a complex non-centrosymmetric cubic structure in space group  $P-43m$  with cell parameter  $a = 12.6881(8)$  Å. The structure of  $\text{Ba}_{10}\text{Ti}_{24}\text{Bi}_{39}$  solved by our single crystal crystallographic study and projected along the  $c$ -axis is depicted in Figure 1(b). This structure is very similar to that of  $\text{Ba}_5\text{Ti}_{12}\text{Sb}_{19+x}$  ( $x \leq 0.2$ ) reported earlier since  $\text{Ba}_5\text{Ti}_{12}\text{Sb}_{19+x}$  ( $x \leq 0.2$ ) can also be denoted by  $\text{Ba}_{10}\text{Ti}_{24}\text{Sb}_{38+x}$  ( $x \leq 0.4$ ).[41] The atomic positions and the occupancies of most atoms, excluding the variable-amount Bi/Sb atom, in the two materials are almost the same. In the center of the cubic unit cell of  $\text{Ba}_{10}\text{Ti}_{24}\text{Bi}_{39}$ , six Ba(2) atoms, four Bi(2) atoms and twelve Bi(4) atoms form a cage-like structure which has one Bi(6) atom encapsulated inside, as shown in Figure 1(c). The distances from the center of the cage to the Ba(2), Bi(2) and Bi(4) atoms are  $4.100(3)$  Å,  $3.8984(10)$  Å and  $5.0686(7)$  Å respectively. These are longer than the regular Ba-Bi and Bi-Bi bonding distances, so the Bi(6) atom is not stable sitting precisely at the center position. Instead, Bi(6) adopts a positional disorder, similar to disordered guests in cage-like structures of hydrogen clathrate hydrates and some inorganic clathrates.[42,43] Specific to  $\text{Ba}_{10}\text{Ti}_{24}\text{Bi}_{39}$ , the Bi(6) site splits into Bi(6) and Bi(6)' and the displacement factors of Bi(6) site are relatively large, as exhibited in the ellipsoid model in the top panel of Figure 1(d). The electron density distribution generated by Fourier transform from the single-crystal diffraction data is presented in the bottom panel of Figure 1(d) reflecting the real space distribution of the Bi(6) atoms. The total number of Bi(6) atoms in

one unit cell based on the occupancy of Bi(6) and Bi(6)' is 1, suggesting that all the cages in the structure of  $\text{Ba}_{10}\text{Ti}_{24}\text{Bi}_{39}$  are filled. The differences between the structures of  $\text{Ba}_{10}\text{Ti}_{24}\text{Bi}_{39}$  and  $\text{Ba}_5\text{Ti}_{12}\text{Sb}_{19+x}$  are mainly on features of guest atoms. Unlike the split position, the disordered distribution and the 100% occupancy of Bi(6) guest atoms in  $\text{Ba}_{10}\text{Ti}_{24}\text{Bi}_{39}$ , only few of cages in  $\text{Ba}_5\text{Ti}_{12}\text{Sb}_{19+x}$  are filled by guest atoms and in the filled cages the Sb(6) guest atoms occupy only the site (0.6354(5), 0.6354(5), 0.6354(5)) locally,[41] a site like Bi(6)' but closer to the facets of the polyhedral cage. This indicates the significantly smaller cage in  $\text{Ba}_5\text{Ti}_{12}\text{Sb}_{19+x}$  can be self-stabilizing without guest atoms.

A striking feature of  $\text{Ba}_{10}\text{Ti}_{24}\text{Bi}_{39}$  is the Ti sublattice which is built up of a three-dimensional network of intersecting Kagome-lattice-like structure fragments, see Figure 2(a). As shown in Figure 2(b), the fragment units (indicated in the red circle) connect to each other by sharing Ti(2) atoms to form an infinite three-dimensional network. It is known that Kagome-lattice-type configuration of magnetic atoms, as shown in Figure 2(c), will lead to magnetic frustration or multiple competing magnetic interactions in the lattice.[44] The three-dimensional network of intersecting Kagome-lattice-like fragments in  $\text{Ba}_{10}\text{Ti}_{24}\text{Bi}_{39}$  may also bring on unusual magnetic properties in this material as we discuss below.

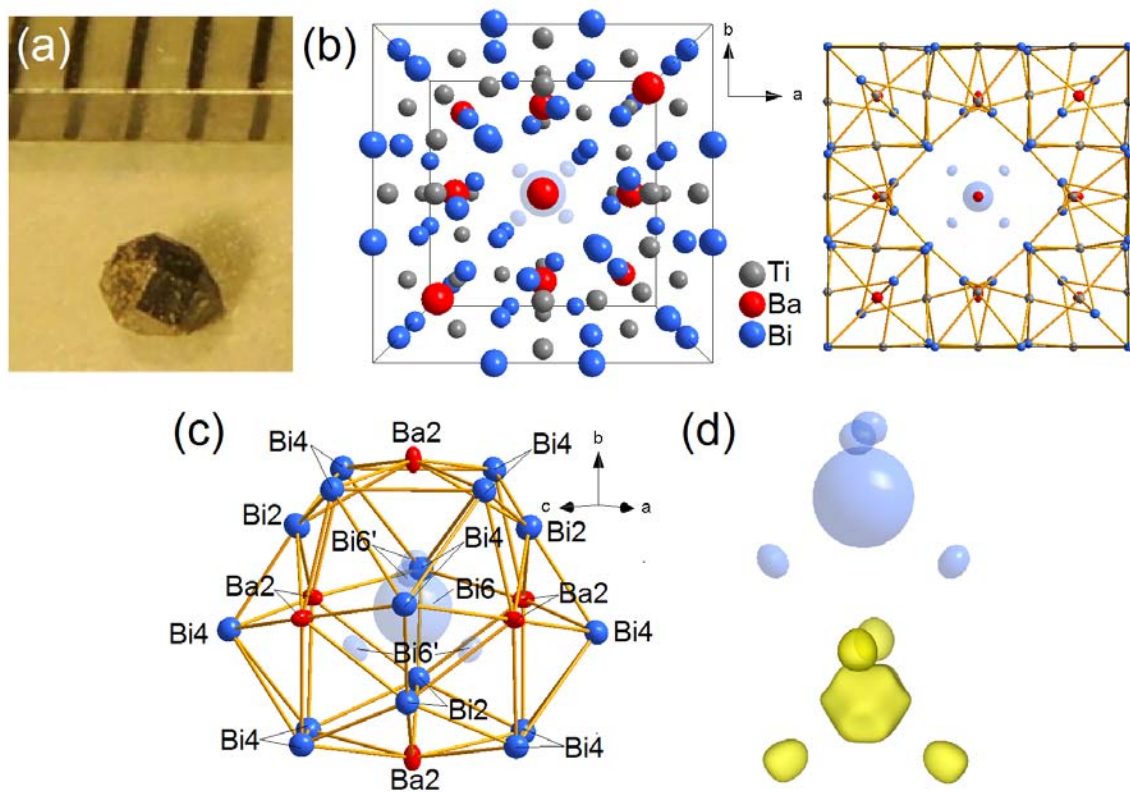


**Figure 1.** (a) Photograph of a typical  $\text{Ba}_{10}\text{Ti}_{24}\text{Bi}_{39}$  crystal. (b) Crystal structure of  $\text{Ba}_{10}\text{Ti}_{24}\text{Bi}_{39}$ . (c) Cage-like structure composed of Ba(2), Bi(2), and Bi(4) atoms with one Bi(6) atom encapsulated inside. (d) Ellipsoid representation of Bi(6) and Bi(6)' (top), and the electron density distribution generated by Fourier transform from the single-crystal diffraction data (bottom).

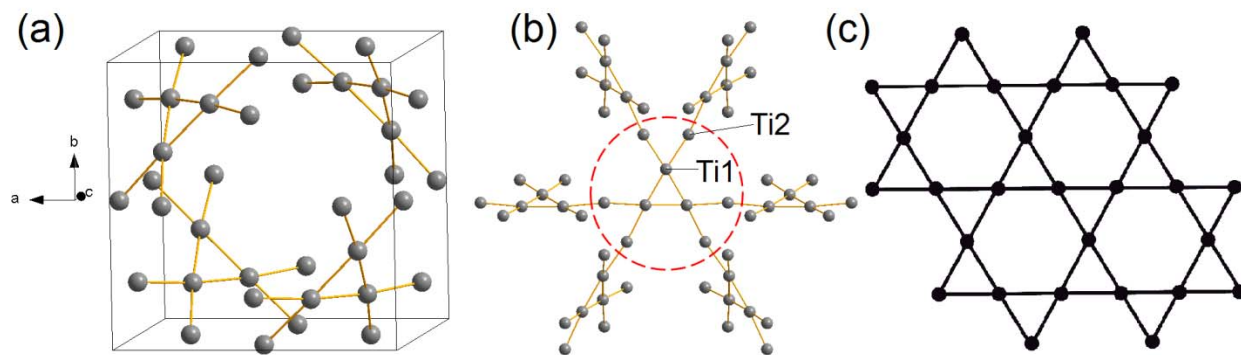


**Figure 2.** (a) Ti sublattice in the structure of  $\text{Ba}_{10}\text{Ti}_{24}\text{Bi}_{39}$ . (b) Kagome-lattice-like structure fragment (in the red circle) in the Ti sublattice of  $\text{Ba}_{10}\text{Ti}_{24}\text{Bi}_{39}$  and how they connect. (c) Classic Kagome lattice.

**Magnetic Properties.** Magnetic susceptibility of  $\text{Ba}_{10}\text{Ti}_{24}\text{Bi}_{39}$  shows a very weak temperature dependence, see Figure 3. The magnetizations versus fields at different temperatures are almost linear up to 7 T as shown in the inset of Figure 3. There is a tiny magnetic hysteresis loop at low magnetic fields at 10 K, indicating a very small amount of ferromagnetic impurities in the sample, see Figure S4 in SM.[34] However, this will not affect the magnetic susceptibility data measured at high magnetic fields ( $\mu_0 H = 5$  T). The upturn below 14 K is probably due to paramagnetic impurities or defects in the sample. It does not show a Curie-Weiss law from 15 to 300 K. The almost linear temperature-dependent magnetic susceptibility with a positive slope in  $\text{Ba}_{10}\text{Ti}_{24}\text{Bi}_{39}$ , possibly originating from the three-dimensional network of intersecting Kagome-lattice-like fragments in  $\text{Ba}_{10}\text{Ti}_{24}\text{Bi}_{39}$ , is similar to the cases in the high-temperature iron-based superconducting parent compounds which are believed to be due to antiferromagnetic fluctuations above the spin density wave transition in those compounds.[45] However, there is no magnetic order detected in  $\text{Ba}_{10}\text{Ti}_{24}\text{Bi}_{39}$  below room temperature. The relative change in magnetic susceptibility from 300 to 50 K in  $\text{Ba}_{10}\text{Ti}_{24}\text{Bi}_{39}$  is only 12%, which can also be interpreted by a dominant temperature-independent Pauli paramagnetism of the sample supported by DFT calculations shown below with some unknown antiferromagnetic contributions. We have also performed magnetic susceptibility measurements on another crystal (sample A1) grown under a different condition, the result of which shows exactly the same temperature-dependent behavior, see the data in SM.[34] The origin of the almost linear temperature-dependent magnetic susceptibility in  $\text{Ba}_{10}\text{Ti}_{24}\text{Bi}_{39}$  is unclear and likely due to the unusual magnetic interaction in the three-dimensional network of intersecting Kagome-lattice-like fragments. Further investigations will be needed to elucidate this issue which is outside of the scope of this report.

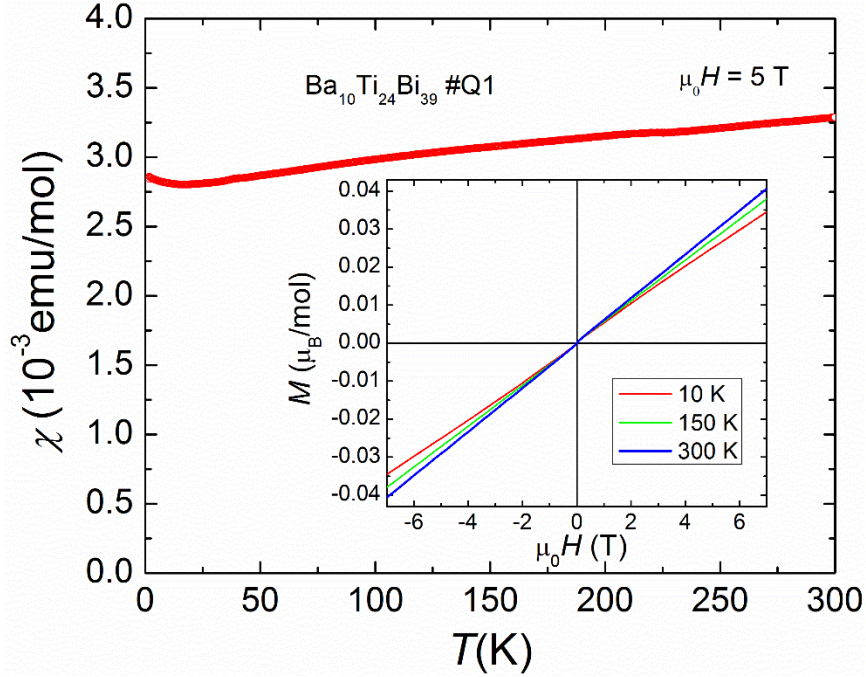


**Figure 3.** (a) Temperature dependences of magnetic susceptibility measured at  $\mu_0 H = 5$  T for single-crystalline  $\text{Ba}_{10}\text{Ti}_{24}\text{Bi}_{39}$  sample Q1. Inset shows isothermal magnetizations at 10, 150 and 300 K.

**Resistivity and Magnetoresistance.** The electrical resistivity for  $\text{Ba}_{10}\text{Ti}_{24}\text{Bi}_{39}$  as a function of temperature is displayed in the main frame of Figure 4(a). The resistivity has a high residual value  $\rho_0$  at 2 K and the residual resistivity ratio (RRR) was calculated to be 1.72 which is very small for a single crystal sample. This reflects an extremely strong transport scattering in this material. The strong charge transport scattering can be attributed to the complexity of disorder in the structure, particularly the disorder of the guest atoms. Above 25 K, the resistivity shows an unconventional bow-shaped behavior. This kind of behavior was found in many strongly correlated systems, for instance in  $\text{Rh}_{17}\text{S}_{15}$ ,<sup>[46]</sup>  $\kappa$ -(BEDT-TTF)<sub>2</sub>Cu[N(CN)<sub>2</sub>]Br,<sup>[47]</sup> and  $\text{LiV}_2\text{O}_4$ .<sup>[48]</sup>

We observed a  $T^2$  temperature dependence for the low-temperature part of the resistivity,  $\rho(T) = \rho_0 + AT^2$ , establishing the existence of a well-defined Fermi-liquid state at low temperatures, as shown in the inset of Figure 4(a). From the linear fitting process we obtain  $\rho_0 = 1.000 \text{ m}\Omega\cdot\text{cm}$  and  $A = 0.0885 \text{ }\mu\Omega\cdot\text{cm}/\text{K}^2$ . The coefficient  $A$  for this material is significantly larger than that of simple metals which is typically around  $10^{-5} \text{ }\mu\Omega\cdot\text{cm}/\text{K}^2$ . The significantly enhanced  $A$  greatly increases the contribution of the  $T^2$  term to the resistivity, which causes a fast upturn with the increase of temperature in the low temperature resistivity of  $\text{Ba}_{10}\text{Ti}_{24}\text{Bi}_{39}$ . This is sharply contrasted to the case of simple metals where the resistivity has a flat low-temperature part. As the  $T^2$  term arises from the electron-electron scattering, the  $\text{Ba}_{10}\text{Ti}_{24}\text{Bi}_{39}$  appears to exhibit very large electron-electron scattering below 10 K in its electronic transport.

Magnetoresistance (MR) measurements is what we used as a tool for investigating the properties of electronic scattering.[49,50] Field dependences of magnetoresistance at different temperatures for  $\text{Ba}_{10}\text{Ti}_{24}\text{Bi}_{39}$  are shown in Figure 4(b). We find the magnetoresistance significantly varies with temperature and magnetic field. At 300 K the magnetoresistance rises steadily with magnetic field with no signs of saturation. However, at 275 K the magnetoresistance rises from 0 to 5 T but then saturates above 5 T. At lower temperatures the magnetoresistance rises first and then undergoes a broad maximum at moderate fields followed by a falling at higher fields. At 10 K it reaches a broad maximum at very low field and then decreases quickly; at 6 T the magnetoresistance drops to 0 and has a sign reversal from positive to negative. A similar MR behavior was also observed in other crystals from the same batch, see Figure S9 in SM[34]. We suggest the magnetoresistance behavior can be explained with a mixture of two competing components one positive and the other negative. At low temperatures the

contributions of the two components are comparable while at high temperatures the positive component dominates and the negative component is diminished. The negative MR component is probably due to weak localization[51] from the significant disorder in this material as proved above. The relative contributions of positive and negative components in MR vary in different crystals due to the possibly different defect distributions in those crystals.

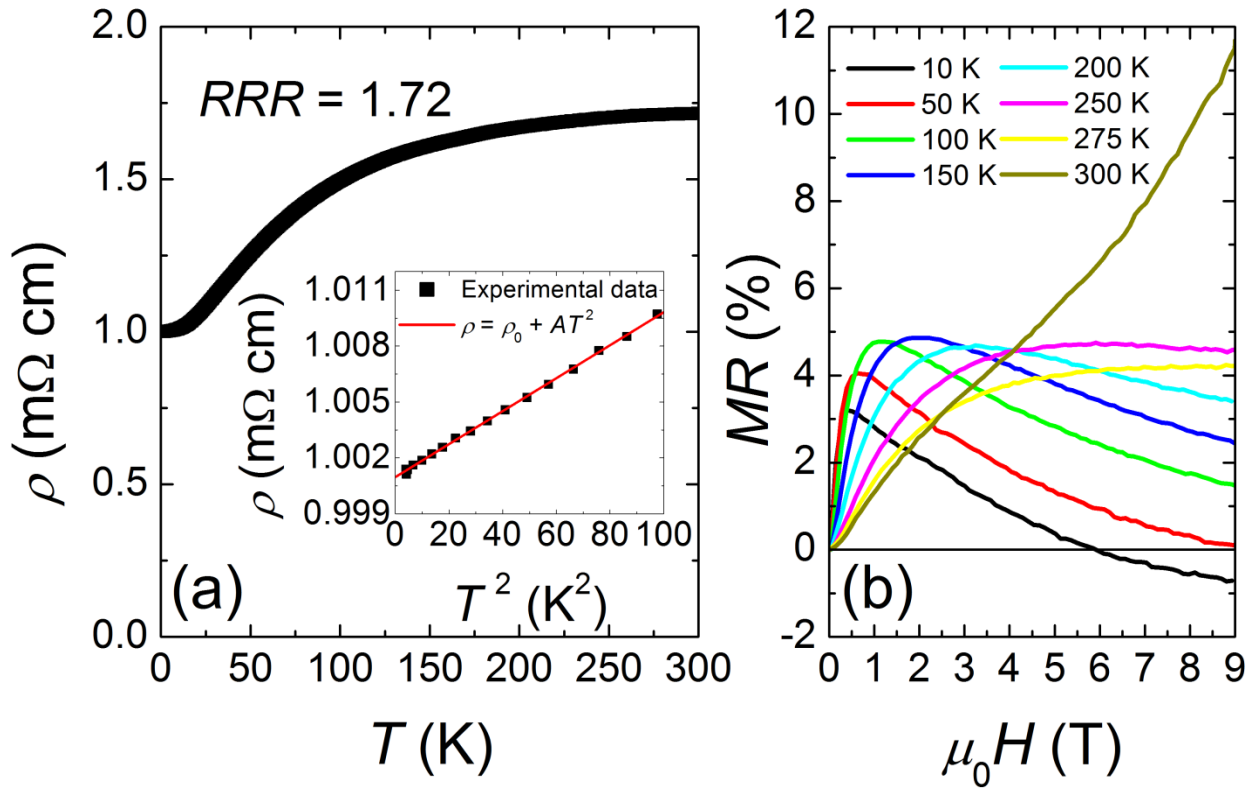


**Figure 4.** (a) Main frame: temperature dependence of resistivity for  $\text{Ba}_{10}\text{Ti}_{24}\text{Bi}_{39}$ . Inset: power-law fitting to the low-temperature part of resistivity. (b) Field dependence of magnetoresistance (MR) at different temperatures for  $\text{Ba}_{10}\text{Ti}_{24}\text{Bi}_{39}$ . At 10 K the MR undergoes a positive-to-negative sign reversal.

**Specific Heat.** Specific heat measurements for  $\text{Ba}_{10}\text{Ti}_{24}\text{Bi}_{39}$  were performed from 2 to 300 K, Figure 5(a). No peaks or jumps associated with structural or magnetic transitions were observed. At 300 K, the specific heat approaches the value of  $3NR$ , the so-called Dulong-Petit limit, where  $N = 73$  (the number of atoms in the

chemical formula) and  $R = 8.314 \text{ J}\cdot\text{mol}^{-1}\cdot\text{K}^{-1}$  (the gas constant). This is consistent with the stoichiometry and suggests there are no massive vacancies in the structure. As predicted by Fermi-liquid theory, at very low temperatures, the specific heat  $C$  is approximate to the sum of the first term of phonon specific heat  $\beta T^3$  and the first term of electronic specific heat  $\gamma T$ . In other words, the  $C/T$  versus  $T^2$  curve follows a linear relationship  $C/T = \gamma + \beta T^2$  at low temperatures, as shown in the inset of Figure 2(b). From linear fitting, we can estimate the electronic specific heat coefficient  $\gamma$  to be  $100.2 \text{ mJ}\cdot\text{mol}^{-1}\cdot\text{K}^{-2}$  and the phonon specific heat coefficient  $\beta$  to be  $40.73 \text{ mJ}\cdot\text{mol}^{-1}\cdot\text{K}^{-4}$ .

Taking the value of  $\beta$  into the formula  $\Theta_D = (12\pi^4 NR/5\beta)^{1/3}$ , we obtain a Debye temperature  $\Theta_D$  of 151.6 K for  $\text{Ba}_{10}\text{Ti}_{24}\text{Bi}_{39}$  which is very close to those of other bismuth-rich compounds. According to the band structure calculations to be discussed in the next subsection, the conductive electrons in this system are provided by all the Ti and Bi atoms. Therefore, we can distribute the value of  $\gamma$  to each Ti or Bi atom, so that  $\gamma$  equals  $1.590 \text{ mJ}\cdot\text{mol}^{-1}\cdot\text{K}^{-2}$  for per mole Ti or Bi atoms. Using the coefficient  $A$  obtained in the fitting of the resistivity, we can calculate the Kadowaki-Woods ratio  $A/\gamma^2$ , which is the criterion for the strength of electron-electron scattering,[52] for the present material to be  $35 \mu\Omega\cdot\text{cm}\cdot\text{mol}^2\cdot\text{K}^2\cdot\text{J}^{-2}$ .

For simple metals the ratio  $A/\gamma^2$  is typically a constant,[53] while it is significantly enhanced for heavy-fermion materials, which is firstly raised by K. Kadowaki and S. B. Woods.[52] The  $A/\gamma^2$  has become known as the Kadowaki-Woods ratio and its magnitude is regarded as a measure for the strength of electron-electron scattering in materials.[54,55]

To compare the Kadowaki-Woods ratio for  $\text{Ba}_{10}\text{Ti}_{24}\text{Bi}_{39}$  with other materials, we add the data of  $\text{Ba}_{10}\text{Ti}_{24}\text{Bi}_{39}$  into the standard Kadowaki-Woods plot, Figure 5(b).

This plot was introduced in Reference [56] and contains data for different transition metals, heavy-fermion materials, and other systems with a large Kadowaki-Woods ratio. From Figure 5(b), we can see the data for the transition metals and the heavy-fermion materials respectively fall on two separate lines, which represents the universal relationships of the Kadowaki-Woods ratio for simple metals and heavy-fermion materials. The point for  $\text{Ba}_{10}\text{Ti}_{24}\text{Bi}_{39}$  is located well above the two lines indicating the Kadowaki-Woods ratio for this compound is very large. From the data presented in the standard Kadowaki-Woods plot,[56] we find the Kadowaki-Woods ratio for  $\text{Ba}_{10}\text{Ti}_{24}\text{Bi}_{39}$  is among the largest values observed in materials.

The giant Kadowaki-Woods ratio reveals the electron-electron scattering in  $\text{Ba}_{10}\text{Ti}_{24}\text{Bi}_{39}$  is enormous. Different from the case in the heavy-fermion materials, the enormous electron-electron scattering in  $\text{Ba}_{10}\text{Ti}_{24}\text{Bi}_{39}$  does not have  $f$  electrons and no Kondo physics involved. This possibly suggests an unprecedented origin for the enormous electron-electron scattering in intermetallics.

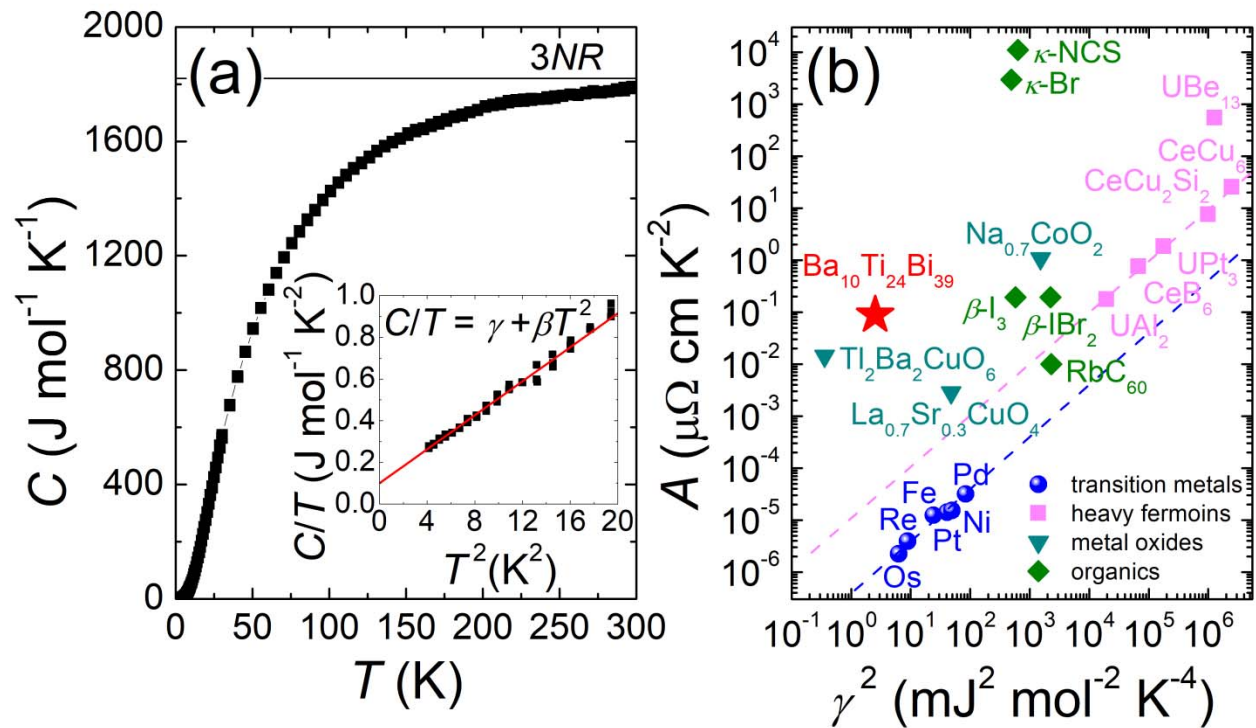


**Figure 5.** (a) Main frame: temperature dependence of specific heat for  $\text{Ba}_{10}\text{Ti}_{24}\text{Bi}_{39}$ . Inset: specific heat divided by temperature  $C/T$  as a function of  $T^2$ . Red line shows a linear fit to the low-temperature part of the  $C/T$  versus  $T^2$  curve. The slope and intercept of the red line represent  $\beta$  and  $\gamma$  respectively. (c) The standard Kadowaki-Woods plot. In labelling the data points we use the following abbreviations:  $\kappa\text{-Br}$  is  $\kappa\text{-(BEDT-TTF)}_2\text{Cu}[\text{N}(\text{CN})_2]\text{Br}$ ;  $\kappa\text{-NCS}$  is  $\kappa\text{-(BEDT-TTF)}_2\text{Cu}(\text{NCS})_2$ ;  $\beta\text{-I}_3$  is  $\beta\text{-(BEDT-TTF)}_2\text{I}_3$ ; and  $\beta\text{-IBr}_2$  is  $\beta\text{-(BEDT-TTF)}_2\text{IBr}_2$ .

**Band Structure.** To better understand the magnetic and electronic properties of  $\text{Ba}_{10}\text{Ti}_{24}\text{Bi}_{39}$ , we calculated the electronic band structure using first-principles density functional theory. As shown in Figure 6(a), there are several bands crossing the Fermi energy making the system a metal which is consistent with the experimental results.

When the large spin-orbital coupling (SOC) effect of Bi atoms is taken into account the electronic structure of  $\text{Ba}_{10}\text{Ti}_{24}\text{Bi}_{39}$  is shown in Figure 6(b). Comparing with the band structure without considering SOC, the bands near the Fermi energy are split by the SOC effect. After the band splitting, more bands cross the Fermi level and lead to a more complicated band structure, which indicates the SOC effect cannot be neglected in this compound. The SOC effect kills the hole pocket at the  $\Gamma$  point and brings up more small Fermi pockets. The system is still a metal after considering SOC because several bands cross the Fermi level. The bands near the Fermi energy are split by the SOC effect and hybridize again, thus forming a very complicated Fermi surface. From Figure 6(b), we can see that a few of electron and hole pockets coexist. The electronic specific heat coefficient  $\gamma$  is calculated  $194 \text{ mJ}\cdot\text{mol}^{-1}\cdot\text{K}^{-2}$  which is consistent with the experimental one.

As shown in Figure 7(a), there is a peak in the density of states (DOS) at the Fermi level when SOC not considered. This suggests the possibility of Stoner instability[57] against ferromagnetism (FM). However, after performing a spin polarized calculation using GGA+SOC with initial FM setup we found that it

converges to a non-magnetic-order ground state. The peak at the Fermi level is also removed after turning on SOC for the calculations, see Figure 7(b).

Figure 7(b) and 7(c) present the total and atomic DOS when SOC considered. We can see all the Bi and Ti atoms contribute to the total DOS of the system. Compared with the Bi-6*p* electrons, the Ti-3*d* electrons are more dominated. However, differently from other Bi atoms, the Bi(6) atom in the cage gives the highest DOS at the Fermi level among all atoms. We suggest the enormous electron-electron scattering in Ba<sub>10</sub>Ti<sub>24</sub>Bi<sub>39</sub> arises from the complex multiband hybridization near the Fermi surface. The random distribution of the Bi(6) atom may play an important role since the Bi(6) atom gives the highest proportion in the DOS at the Fermi level.

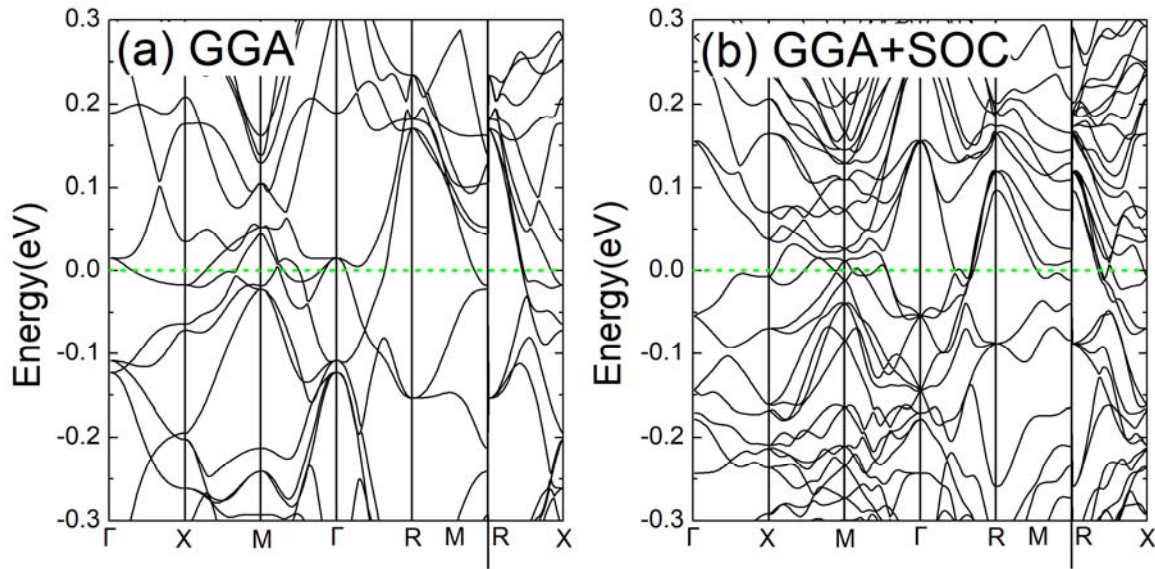


**Figure 6.** Band structures along the high symmetric points in the reduced Brillouin zone calculated by GGA (a) without and (b) with considering SOC. The horizontal green dashed lines refer to the Fermi energy level.

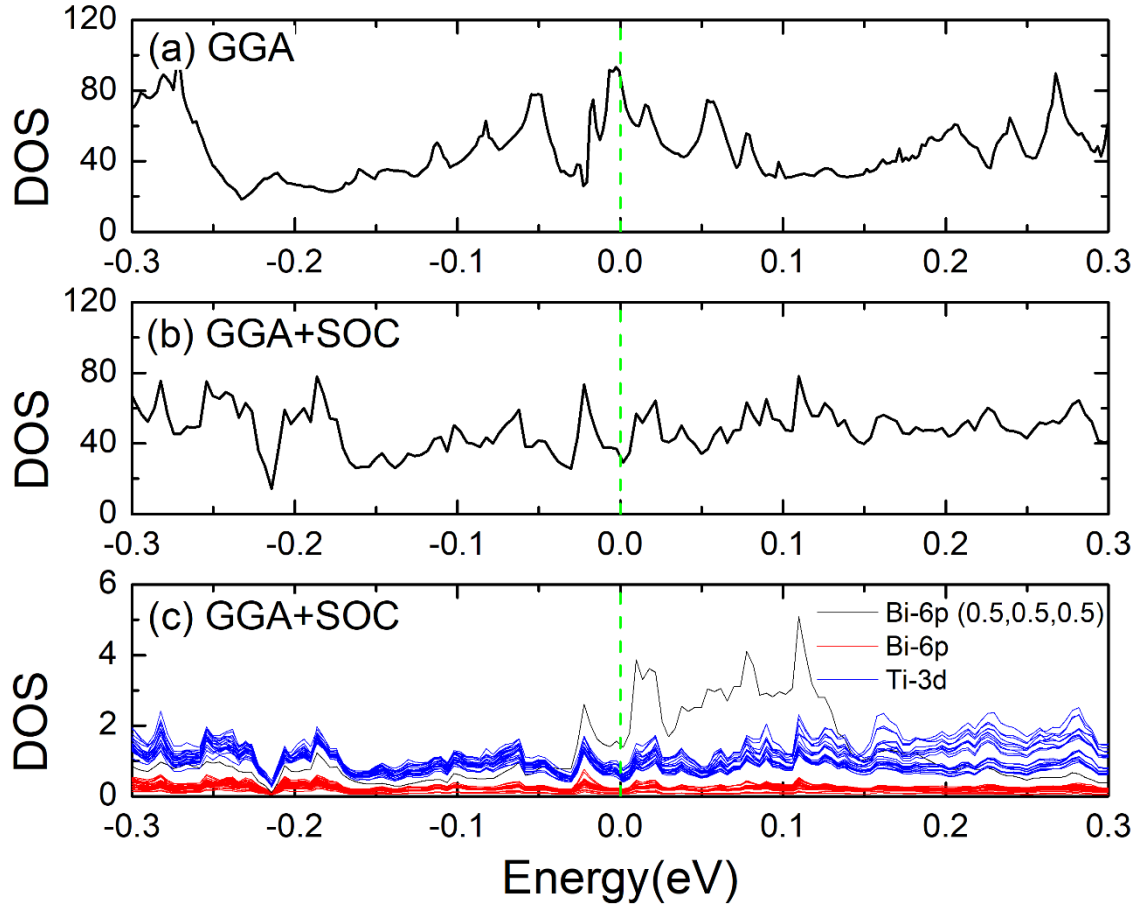


**Figure 7.** (a) Total density of states (DOS) at around the Fermi energy level without SOC considered. (b) Total DOS with SOC considered. (c) Atomic orbital projected DOS with SOC considered. The vertical green dashed lines refer to the Fermi energy level.

## CONCLUSIONS

The cubic non-centrosymmetric compound  $\text{Ba}_{10}\text{Ti}_{24}\text{Bi}_{39}$  has a filled-cage structure with guest atoms distributing randomly in the cages. It shows a positive temperature-dependent coefficient in the magnetic susceptibility, the origin of which needs further investigations. The magnetoresistance at low temperatures has a positive to negative crossover with increasing the magnetic fields, indicating a two competing factors in determining the transport properties. The complex multiband hybridization of the abundant of Ti and Bi atoms near the Fermi surface may play a role in the enormous electron-electron scattering in this material, which

is revealed by the large Kadowaki-Woods ratio among the top ones for intermetallics.

## **ACKNOWLEDGMENT**

We thank Dr Daniel Phelan for help with the magnetic susceptibility measurements. This work was supported by the U.S. Department of Energy, Office of Science, Basic Energy Sciences, Materials Sciences and Engineering Division. Use of the Center for Nanoscale Materials, an Office of Science user facility, was supported by the U.S. Department of Energy, Office of Science, Office of Basic Energy Sciences, under Contract No. DE-AC02-06CH11357. Band structure calculations done at Nanjing University (by Y. Du and X. Wan) are supported by the NSF of China (Grant Nos. 11374137 and 11525417).

## REFERENCE

- [1] M. Z. Hasan and C. L. Kane, *Rev. Mod. Phys.* **82**, 3045 (2010).
- [2] X. L. Qi and S. C. Zhang, *Rev. Mod. Phys.* **83**, 1057 (2011).
- [3] X. Zhu, H. Lei, C. Petrovic, and Y. Zhang, *Phys. Rev. B* **86**, 024527 (2012).
- [4] M. Sturza, F. Han, C. D. Malliakas, D. Y. Chung, H. Claus, and M. G. Kanatzidis, *Phys. Rev. B* **89**, 054512 (2014).
- [5] S. K. Kushwaha, J. W. Krizan, J. Xiong, T. Klimczuk, Q. D. Gibson, T. Liang, N. P. Ong, and R. J. Cava, *J. Phys. Condens. Matter* **26**, 212201 (2014).
- [6] N. Haldolaarachchige, S. K. Kushwaha, Q. Gibson, and R. J. Cava, *Supercond. Sci. Tech.* **27**, 105001 (2014).
- [7] Z. K. Liu, B. Zhou, Y. Zhang, Z. J. Wang, H. M. Weng, D. Prabhakaran, S. K. Mo, Z. X. Shen, Z. Fang, and X. Dai, *Science* **343**, 864 (2014).
- [8] S. Y. Xu, C. Liu, S. K. Kushwaha, R. Sankar, J. W. Krizan, I. Belopolski, M. Neupane, G. Bian, N. Alidoust, and T. R. Chang, *Science* **347**, 294 (2015).
- [9] Z. Wang, Y. Sun, X.-Q. Chen, C. Franchini, G. Xu, H. Weng, X. Dai, and Z. Fang, *Phys. Rev. B* **85**, 195320 (2012).
- [10] J. Park, G. Lee, F. Wolff-Fabris, Y. Y. Koh, M. J. Eom, Y. K. Kim, M. A. Farhan, Y. J. Jo, C. Kim, and J. H. Shim, *Phys. Rev. Lett.* **107**, 126402 (2011).
- [11] J. K. Wang, L. L. Zhao, Q. Yin, G. Kotliar, M. Kim, M. Aronson, and E. Morosan, *Phys. Rev. B* **84**, 064428 (2011).
- [12] K. Wang, D. Graf, H. Lei, S. W. Tozer, and C. Petrovic, *Phys. Rev. B* **84**, 220401 (2011).
- [13] K. Wang, D. Graf, L. Wang, H. Lei, S. W. Tozer, and C. Petrovic, *Phys. Rev. B* **85**, 041101 (2012).
- [14] L. Li, K. Wang, D. Graf, L. Wang, A. Wang, and C. Petrovic, *Phys. Rev. B* **93**, 115141 (2016).
- [15] K. Wang, D. Graf, and C. Petrovic, *Phys. Rev. B* **87**, 235101 (2013).
- [16] M. Sakano, K. Okawa, M. Kanou, H. Sanjo, T. Okuda, T. Sasagawa, and K. Ishizaka, *Nat. Comm.* **6**, 8595 (2015).
- [17] Y. Nakajima, R. Hu, K. Kirshenbaum, A. Hughes, P. Syers, X. Wang, K. Wang, R. Wang, S. R. Saha, D. Pratt, J. W. Lynn, and J. Paglione, *Sci. Adv.* **1**, e1500242 (2015).
- [18] F. F. Tafti, Q. Gibson, S. Kushwaha, J. W. Krizan, N. Haldolaarachchige, and R. J. Cava, *Proc. Natl. Acad. Sci. U.S.A.*, E3475 (2016).
- [19] S. Sun, Q. Wang, P.-J. Guo, K. Liu, and H. Lei, *New J. Phys.*, 082002 (2016).
- [20] N. Kumar, C. Shekhar, S.-C. Wu, I. Leermakers, O. Young, U. Zeitler, B. Yan, and C. Felser, *Phys. Rev. B* **93**, 241106 (2016).
- [21] U. Schwarz, S. Tencé, O. Janson, C. Koz, C. Krellner, U. Burkhardt, H. Rosner, F. Steglich, and Y. Grin, *Angew. Chem. Int. Ed.* **52**, 9853 (2013).
- [22] S. M. Clarke, J. P. Walsh, M. Amsler, C. D. Malliakas, T. Yu, S. Goedecker, Y. Wang, C. Wolverton, and D. E. Freedman, *Angew. Chem. Int. Ed.* **55**, 13446 (2016).
- [23] F. Han, C. D. Malliakas, C. C. Stoumpos, M. Sturza, H. Claus, D. Y. Chung, and M. G. Kanatzidis, *Phys. Rev. B* **88**, 144511 (2013).
- [24] R. Retzlaff, A. Buckow, P. Komissinskiy, S. Ray, S. Schmidt, H. Mühlig, F. Schmidl, P. Seidel, J. Kurian, and L. Alff, *Phys. Rev. B* **91**, 104519 (2015).
- [25] F. Han, X. Wan, D. Phelan, C. C. Stoumpos, M. Sturza, C. D. Malliakas, Q. a. Li, T. H. Han, Q. Zhao, and D. Y. Chung, *Phys. Rev. B* **92**, 045112 (2015).

- [26] X. Lin, W. E. Straszheim, S. L. Bud'ko, and P. C. Canfield, *J. Alloys Compd.* **554**, 304 (2013).
- [27] E. M. Seibel, W. Xie, Q. D. Gibson, and R. J. Cava, *J. Solid State Chem.* **230**, 318 (2015).
- [28] C. B. R. Jesus, M. M. Piva, P. F. S. Rosa, C. Adriano, Z. Fisk, and P. G. Pagliuso, *Phys. Procedia* **75**, 618 (2015).
- [29] J. P. Walsh, S. M. Clarke, Y. Meng, S. D. Jacobsen, and D. E. Freedman, *ACS Cent. Sci.* (2016).
- [30] A. Ovchinnikov and S. Bobev, *European Journal of Inorganic Chemistry*, 1266 (2018).
- [31] E. Zintl, *Angewandte Chemie* **52**, 1 (1939).
- [32] A. K. Misra, *Metallurgical Transactions A* **22**, 715 (1991).
- [33] S. Amano, D. Bogdanovski, H. Yamane, M. Terauchi, and R. Dronskowski, *Angewandte Chemie International Edition* **55**, 1652 (2016).
- [34] See Supplemental Materials at XXX where SEM picture and element analysis, X-ray crystallographic data (CIF), tables for detailed structure parameters, detailed magnetic susceptibility data from two different crystals and resistivity data from another crystal are provided.
- [35] C. Stoe, Stoe & Cie, Darmstadt, Germany (2002).
- [36] G. M. Sheldrick, *Acta Cryst. A* **64**, 112 (2008).
- [37] G. Kresse and J. Hafner, *Phys. Rev. B* **48**, 13115 (1993).
- [38] G. Kresse and D. Joubert, *Phys. Rev. B* **59**, 1758 (1999).
- [39] J. P. Perdew, K. Burke, and M. Ernzerhof, *Phys. Rev. Lett.* **77**, 3865 (1996).
- [40] D. Koelling and B. Harmon, *J. Phys. C* **10**, 3107 (1977).
- [41] H. Bie and A. Mar, *J. Solid State Chem.* **182**, 3131 (2009).
- [42] T. A. Strobel, K. C. Hester, E. D. Sloan, and C. A. Koh, *J. Am. Chem. Soc.* **129**, 9544 (2007).
- [43] H. Zhang, H. Borrmann, N. Oeschler, C. Candolfi, W. Schnelle, M. Schmidt, U. Burkhardt, M. Baitinger, J. T. Zhao, and Y. Grin, *Inorg. Chem.* **50**, 1250 (2011).
- [44] B. Fåk, E. Kermarrec, L. Messio, B. Bernu, C. Lhuillier, F. Bert, P. Mendels, B. Koteswararao, F. Bouquet, and J. Ollivier, *Physical review letters* **109**, 037208 (2012).
- [45] G. M. Zhang, Y. H. Su, Z. Y. Lu, Z. Y. Weng, D. H. Lee, and T. Xiang, *EPL (Europhysics Letters)* **86**, 37006 (2009).
- [46] H. R. Naren, A. Thamizhavel, A. K. Nigam, and S. Ramakrishnan, *Phys. Rev. Lett.* **100**, 026404 (2008).
- [47] C. Strack, C. Akinci, V. Pashchenko, B. Wolf, E. Uhrig, W. Assmus, M. Lang, J. Schreuer, L. Wiehl, and J. Schlueter, *Physical Review B* **72**, 054511 (2005).
- [48] C. Urano, M. Nohara, S. Kondo, F. Sakai, H. Takagi, T. Shiraki, and T. Okubo, *Physical review letters* **85**, 1052 (2000).
- [49] Q. Li, B. T. Liu, Y. F. Hu, J. Chen, H. Gao, L. Shan, H. H. Wen, A. V. Pogrebnyakov, J. M. Redwing, and X. X. Xi, *Phys. Rev. Lett.* **96**, 167003 (2006).
- [50] H. Yang, Y. Liu, C. Zhuang, J. Shi, Y. Yao, S. Massidda, M. Monni, Y. Jia, X. Xi, and Q. Li, *Phys. Rev. Lett.* **101**, 067001 (2008).
- [51] P. A. Lee and T. V. Ramakrishnan, *Reviews of Modern Physics* **57**, 287 (1985).
- [52] K. Kadowaki and S. Woods, *Solid state communications* **58**, 507 (1986).
- [53] M. Rice, *Physical Review Letters* **20**, 1439 (1968).
- [54] S. Li, L. Taillefer, D. Hawthorn, M. Tanatar, J. Paglione, M. Sutherland, R. Hill, C. Wang, and X. Chen, *Physical review letters* **93**, 056401 (2004).

- [55] T. Park, V. Sidorov, J. Sarrao, and J. Thompson, Physical review letters **96**, 046405 (2006).
- [56] A. Jacko, J. Fjærestad, and B. Powell, Nature Physics **5**, 422 (2009).
- [57] E. C. Stoner, Proc. R. Soc. A **154**, 656 (1936).